Crystal Structure of Human Glutathione *S*-Transferase A3-3 and Mechanistic Implications for Its High Steroid Isomerase Activity[†,‡]

Yijun Gu,[§] Jianxia Guo,[||] Ajay Pal,[||,⊥] Su-Shu Pan,[||] Piotr Zimniak,[#] Shivendra V. Singh,[||] and Xinhua Ji*[,§]

Macromolecular Crystallography Laboratory, National Cancer Institute, Frederick, Maryland 21702, Department of Pharmacology and University of Pittsburgh Cancer Institute, University of Pittsburgh School of Medicine, Pittsburgh, Pennsylvania 15260, and Department of Pharmacology and Toxicology, University of Arkansas for Medical Sciences, and Central Arkansas Veterans Healthcare System, Little Rock, Arkansas 72205

Received June 15, 2004; Revised Manuscript Received October 2, 2004

ABSTRACT: The crystal structure of human class alpha glutathione (GSH) *S*-transferase A3-3 (hGSTA3-3) in complex with GSH was determined at 2.4 Å. Despite considerable amino acid sequence identity with other human class alpha GSTs (e.g., hGSTA1-1), hGSTA3-3 is unique due to its exceptionally high steroid double bond isomerase activity for the transformation of Δ^5-androstene-3,17-dione (Δ^5-AD) to Δ^4-androstene-3,17-dione. A comparative analysis of the active centers of hGSTA1-1 and hGSTA3-3 reveals that residues in positions 12 and 208 may contribute to their disparate isomerase activity toward Δ^5-AD. Substitution of these two residues of hGSTA3-3 with the corresponding residues in hGSTA1-1 followed by kinetic characterization of the wild-type and the mutant enzymes supported this prediction. On the basis of our model of the hGSTA3-3·GSH·Δ^5-AD ternary complex and available biochemical data, we propose that the thiolate group of deprotonated GSH (GS^-) serves as a base to initiate the reaction by accepting a proton from the steroid and the nonionized hydroxyl group of catalytic residue Y9 (HO−Y9) functions as part of a proton-conducting wire to transfer a proton back to the steroid. Residue R15 may function to stabilize the deprotonated thiolate group of GSH (GS^-), and a GSH-bound water molecule may donate a hydrogen bond to the 3-keto group of Δ^5-AD and thus help the thiolate of GS^- to initiate the proton transfer and the subsequent stabilization of the reaction intermediate.

Glutathione *S*-transferases (GSTs,[1] EC 2.5.1.18) play an important role in the detoxification of a wide variety of xenobiotics containing an electrophilic center primarily by catalyzing their conjugation with glutathione (GSH) (*1*, *2*). The catalytic diversity of this family of detoxification enzymes arises, in part, from the existence of at least 14 distinct gene classes: alpha, beta, delta, kappa, lambda, mu, omega, phi, pi, sigma, theta, tau, zeta, and microsomal GSTs (*1*, *2*). Although GST isozymes of each class exhibit relatively broad substrate selectivity, most have unique catalytic attributes that are important in defining their physiological roles (*1*, *3*−*6*). Recent determination of many three-dimensional structures of GSTs (*1*, *7*) has broadened our understanding of the catalytic properties and enzyme−substrate interactions. In addition to their roles in detoxification reactions, GSTs are involved in other biological functions, such as the production of steroid hormones (*8*).

Biosynthesis of steroidal hormones such as testosterone and progesterone proceeds with multiple steps involving oxidation and isomerization reactions. An enzyme with high double bond isomerase activity was originally discovered in bacteria (*9*), but the corresponding isomerase has not been found in mammals. GSTs have been known to exhibit steroid isomerase activity, catalyzing the double bond isomerization of Δ^5-androstene-3,17-dione (Δ^5-AD) and Δ^5-pregnene-3,20-dione (Δ^5-PD), leading to the formation of testosterone and progesterone precursors (*10*). Among different classes of GSTs examined to date, the human class alpha GST isoform with subunit type 3 (hGSTA3-3) is an exceptionally efficient catalyst of double bond isomerization of steroid substrates including Δ^5-AD and Δ^5-PD (*8*) although it shows very low activity toward other substrates such as the model substrate of GSTs, 1-chloro-2,4-dinitrobenzene (*8*). It has also been shown that the exceptional steroid double bond isomerase activity of hGSTA3-3 is dictated by a few active site residues; protein engineering of five residues, which differ between hGSTA2-2 and hGSTA3-3, can introduce high isomerase activity into hGSTA2-2, comparable with that of hGSTA3-3 (*11*).

Previous biochemical data indicated that the deprotonated thiolate group of GSH (GS^-) may serve as a base in the double bond isomerization mechanism and that the non-

[†] This work was supported in part by USPHS Grants CA076348 (to S.V.S.), awarded by the National Cancer Institute, and ES07804 (to P.Z.) and ES009140 (to S.V.S. and P.Z.), awarded by the National Institute of Environmental Health Sciences.

[‡] The atomic coordinates and structure factors have been deposited with the Protein Data Bank under accession code 1TDI.

* Address correspondence to this author. Tel: (301) 846-5035. Fax: (301) 846-6073. E-mail: jix@ncifcrf.gov.

[§] National Cancer Institute.

[||] University of Pittsburgh.

[⊥] Current address: Neopharma Inc.

[#] University of Arkansas for Medical Sciences.

[1] Abbreviations: GSH, glutathione; GST, GSH *S*-transferase; hGSTA1-1, human alpha class GST isoform A1-1; hGSTA3-3, human alpha class GST isoform A3-3; G-site, GSH-binding site; H-site, xenobiotic substrate-binding site; Δ^5-AD, Δ^5-androstene-3,17-dione; Δ^4-AD, Δ^4-androstene-3,17-dione; Δ^5-PD, Δ^5-pregnene-3,20-dione; Δ^4-PD, Δ^4-pregnene-3,20-dione; EA, ethacrynic acid; GSB, *S*-benzylglutathione; GSEa, GSH conjugate of EA; rms, root mean square.

10.1021/bi048757g CCC: $27.50
Published on Web 11/17/2004

ionized hydroxyl group of Y9 (HO−Y9) may assist this reaction and serve as a hydrogen bond donor stabilizing the dienolate intermediate (*8*, *12*, *13*). To elucidate the relationship between the active site structure and the highly efficient isomerase activity of hGSTA3-3 toward Δ^5-AD, we have determined the crystal structure of hGSTA3-3 in complex with GSH. Between hGSTA3-3 and hGSTA1-1, only three active site residues (12, 111, and 208) are different. A structural analysis and comparison of hGSTA3-3 and hGSTA1-1 suggested that residues 12 and 208 might be responsible for their distinct isomerase activity, which was confirmed by kinetic characterization of corresponding single point mutants of hGSTA3-3. A computer model of the hGSTA3-3·GSH·Δ^5-AD ternary complex was built, suggesting that the Y9 hydroxyl functions in a concerted manner with GS^- in proton transfer, during which the GS^- thiolate group accepts a proton from position 4 and the Y9 hydroxyl donates a proton to position 6 of the steroid.

EXPERIMENTAL PROCEDURES

Enzyme Purification and Site-Directed Mutagenesis. The bacterial expression vector pET11a/hGSTA3 was prepared as described previously (*14*); pET30a/hGSTA1 was a generous gift from Dr. Y. C. Awasthi (University of Texas Medical Branch, Galveston, TX) (*15*). Recombinant hGSTA3-3 and hGSTA1-1 were purified as described previously (*14*, *16*). The purity of the recombinant enzyme was ascertained by sodium dodecyl sulfate−polyacrylamide gel electrophoresis prior to the kinetic studies.

The *hGSTA3* cDNA in bacterial expression vector pET11a was subjected to site-directed mutagenesis using the QuickChange site-directed mutagenesis kit (Stratagene, La Jolla, CA). The primers 5′-CCT CAC TAC TTC AAT GCA CGG GGC AGA ATG GAG and 5′-CA GGG AAG CCT CCC ATG GAT GCA AAA GCT TTA G (and their corresponding reverse-complemented primer) were used for G12A and A208M mutations, respectively. The mutated codons are underlined. After confirmation of the sequence, the resulting plasmids were transformed into *Escherichia coli* BL21(DE3) (Novagen, Madison, WI) for protein expression.

Kinetic Measurements. The specific activities of the wild-type hGSTA1-1 and hGSTA3-3 and mutants of hGSTA3-3 for double bond isomerization of Δ^5-AD were determined spectrophotometrically at 30 °C as described by Johansson and Mannervik (*13*) using 100 μM Δ^5-AD and 1 mM GSH. The double bond isomerization of Δ^5-AD was monitored at 248 nm in 25 mM sodium phosphate buffer (pH 8). Kinetic constants were estimated by measuring the isomerase activity as a function of varying Δ^5-AD concentrations (0.5−100 μM) at a fixed concentration of GSH (1 mM).

Crystallization and X-ray Diffraction Data Collection. The hanging drop vapor diffusion technique was used to grow crystals of hGSTA3-3·GSH. The drops contained 10.0% PEG 6000 in 50 mM Na-HEPES buffer (pH 8.0); the protein concentration in the drops was 9.0 mg/mL. No GSH was added to the drop since hGSTA3-3 was purified by GSH affinity chromatography. The drops were equilibrated at 15 °C against the well solution that contains 20% PEG 6000 and 100 mM Na-HEPES (pH 8.0). Diffraction-quality crystals grew within several days.

X-ray diffraction data were collected at 100 K with a DIP2020 area detector mounted on a Rigaku rotating anode X-ray generator using Cu Kα radiation. The crystal belonged to the $P2_1$ space group with unit cell dimensions $a = 92.99$ Å, $b = 95.59$ Å, $c = 114.04$ Å, $\alpha = \gamma = 90.0°$, and $\beta = 90.14°$. The cryoprotectant was 50 mM Na-HEPES (pH8.0), 10% PEG 6000, and 15% glycerol, in which the crystal was annealed for 5 s since the original test showed severe ice rings. The annealed crystal diffracted to 2.4 Å. The distance between the crystal and detector was 115 mm, and the frame size was 0.75°. A total of 210 diffraction images were recorded. The raw data images were processed and scaled using DENZO and SCALEPACK (*17*). Data collection statistics are summarized in Table 1.

Table 1: Data Collection and Structure Refinement Statistics for hGSTA3-3·GSH

	overall	last shell
Data Statistics		
resolution range (Å)	30.0−2.40	2.49−2.40
redundancy	2.38	2.28
completeness (%)	94.7	91.1
$I/\sigma(I)$	9.12	2.94
$R_{scaling}$[a]	0.114	0.355
Refinement Statistics		
completeness with $3\sigma(F)$ cutoff (%)	74.8	50.8
reflections used for refinement	55533	3710
reflections used for R_{free} calculations	2963	221
crystallographic R[b]	0.228	0.259
R_{free}[c]	0.252	0.289
no. of protein atoms/ average B factor (Å^2)	3504/28.1	
no. of ligand (GSH) atoms/ average B factor (Å^2)	40/29.4	
no. of water oxygen atoms/ average B factor (Å^2)	274/32.2	
rms deviations from ideal geometry		
bond distances (Å)	0.01	
bond angles (deg)	1.3	
Ramachandran plot		
most favored ϕ/ψ angles (%)	92.2	
disallowed ϕ/ψ angles (%)	0	

[a] $R_{scaling} = \sum|I - \langle I\rangle|/\sum I$. [b] Crystallographic $R = \sum_{hkl}||F_o| - |F_c||/\sum_{hkl}|F_o|$. [c] Last recorded value.

Crystal Structure Determination and Refinement. The structure of hGSTA3-3·GSH was solved by molecular replacement using AMoRe (*18*). Four dimers were found in the asymmetric unit. The search model was the dimeric molecule of the crystal structure of hGSTA1-1 [PDB code 1GUH (*19*)]. The correlation coefficient and crystallographic R-factor for the solution were 0.70 and 0.41, respectively. Rigid-body refinement within AMoRe (*18*) improved the correlation coefficient and crystallographic R-factor to 0.78 and 0.33, respectively.

The structure refinement was initiated with the CNS package (*20*), using the maximum likelihood target function. A total of 5% reflections were randomly chosen for R_{free} calculations. The B factors of the starting model were adjusted to 5.0−50.0 Å^2. The GSH molecule was temporarily excluded from the refinement. The first round of rigid-body refinement, energy minimization, and grouped B factor refinement resulted in an R_{free} of 0.49 and an R-factor of 0.45 for reflections within 30.0−2.5 Å with $F/\sigma(F) \geq 0$. Maps with the Fourier coefficients $2F_o - F_c$ and $F_o - F_c$ were calculated, revealing the location of the GSH molecule. The second round of refinement was carried out using the simulated annealing strategy (*20*) with strict constraint for

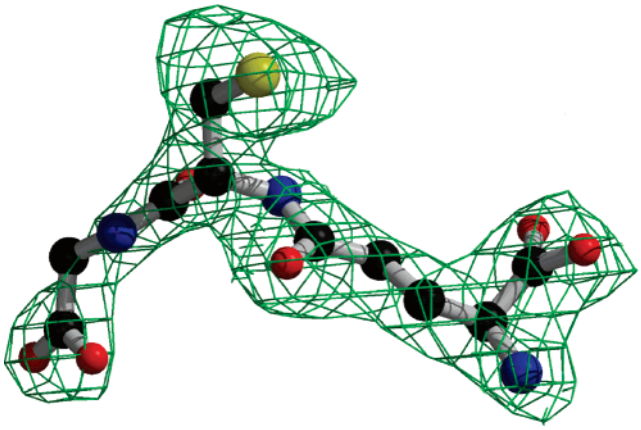

FIGURE 1: Electron density ($2F_o - F_c$ annealed omit map contoured at 1.0σ) for the GSH molecule of the hGSTA3-3·GSH complex. The electron density is shown as a green net, and the GSH molecule is shown as a ball-and-stick model in atomic color scheme (carbon in black, nitrogen in blue, oxygen in red, and sulfur in yellow). The illustration was generated with BobScript (*29*) and Raster3D (*30*).

the eight monomeric hGSTA3-3·GSH complexes in the asymmetric unit. The resulting R_{free} and *R*-factor were 0.34 and 0.33, respectively. The model was checked and adjusted according to the electron density maps and the primary amino acid sequence of hGSTA3-3. Residues with incomplete density were replaced with alanine or glycine. The electron density for the whole model was reasonably good except for the residues at the N- and C-termini. With the progress of the refinement, water molecules were picked from the difference Fourier maps as peaks higher than 3.0σ and were deleted if the *B* factor became higher than 45 Å^2 after being refined. The data for refinement were progressively extended to 2.4 Å. Annealed omit maps were calculated to locate and verify the positions of N- and C-terminal residues, on the basis of which three N-terminal residues and one C-terminal residue were excluded from the model. The GSH and water molecules were also verified with annealed omit maps (Figure 1). When the refinement has reduced the R_{free} and *R*-factor to 0.32 and 0.30, respectively, a dimeric hGSTA3-3·GSH complex was constructed from the monomer using the noncrystallographic symmetry for further refinement. Strict noncrystallographic constraint was used for the four dimeric complexes. Fourteen more rounds of refinement and model adjustment reduced the R_{free} and *R*-factor to 0.26 and 0.23, respectively. The final model contains 3504 protein atoms of two peptides containing residues 4−221, 2 GSH molecules, and 274 oxygen atoms of water molecules. All X-ray diffraction data were included in electron density map calculations, and the program suite O (*21*) was used to check and modify models and to add and delete water molecules. A detailed summary of the crystallographic refinement is shown in Table 1.

Molecular Modeling. Molecular modeling studies were carried out with program suite O (*21*) on an SGI Fuel workstation. The crystal structure of hGSTA3-3·GSH was used as the initial model. The model of Δ^5-AD was built on the basis of Δ^5-androsten-3β-ol-17-one [PDB code 1E3R (*22*)] by replacing the 3-hydroxy group in the A ring with a keto group and docked into the active center of both subunits of hGSTA3-3·GSH, guided by the crystal structure of hGSTA1-1 in complex with the GSH conjugate of ethacrynic acid (EA) [PDB accession code 1GSE (*23*)]. All water molecules in the crystal structure were excluded except for two waters that are hydrogen bonded to GSH (see Discussion for details). The dimeric model of hGSTA3-3·GSH·Δ^5-AD was subjected to energy minimization and geometry optimization with CNS (*24*) using the conjugate gradient method of Powell (*25*) and the geometric parameters of Engh and Hubber (*26*).

RESULTS AND DISCUSSION

Overall Structure of hGSTA3-3·GSH. The final structure has good geometry with reasonable root mean square (rms) deviations (Table 1). As revealed by the protein structure validation program PROCHECK (*27*), 92.2% of the residues exhibit the most favorable $\phi-\psi$ relationships and no residue displays disallowed $\phi-\psi$ values. The N-terminal residues 1−3 and C-terminal residue 222 in both subunits were not included because of the poor electron density.

The overall and domain structures of hGSTA3-3 are very similar to those of other class alpha GSTs, such as hGSTA1-1 [PDB accession codes 1GUH (*19*) and 1GSE (*23*)] and mGSTA1-1 [PDB accession codes 1F3A and 1F3B (*28*)]. Each subunit of hGSTA3-3 is composed of nine α-helices and four β-strands, which are organized into two domains, a smaller N-terminal domain containing a four-stranded β-sheet flanked by three α-helices and a larger C-terminal domain containing six α-helices. The whole model has well-defined electron density.

GSH-Binding Site (G-Site). The GSH molecule is well defined (Figure 1) and assumes the same conformation in both subunits. As established for hGSTA1-1 (*19*), the GSH molecule is bound to the G-site, via hydrogen bonds and/or salt bridges with the surrounding active center residues (not shown), and the thiolate of GSH is within the hydrogen bond distance of the hydroxyl group of the catalytic residue Y9 (Figure 2). Figure 2 depicts the superposition of three crystal structures, including hGSTA3-3·GSH (this work), hGSTA1-1 in complex with *S*-benzylglutathione (GSB) [PDB accession code 1GUH (*19*)], and hGSTA1-1 in complex with the GSH conjugate of EA (GSEa) [PDB accession code 1GSE (*23*)], showing that the GSH moiety is well aligned although the substituent on the sulfur atom of GSH is different in each of the three structures.

Xenobiotic-Binding Site (H-Site). The hGSTA3-3 is homologous to hGSTA1-1 both in primary amino acid sequence (92% identical) and three-dimensional structure (0.36 Å rms deviation for 208 pairs of Cα positions). As expected, the H-site of hGSTA3-3 is highly hydrophobic. It is constructed by the side chains of residues (numbering includes initiator methionine) Y9, F10, G12, R15, L107, L111, A208, L213, A216, F220, and F222 (Figure 2). The H-site residues are conserved in hGSTA1-1 and hGSTA3-3 with three exceptions, amino acid residues in positions 12, 111, and 208: G12, L111, and A208 in hGSTA3-3; and A12, V111, and M208 in hGSTA1-1 (Figure 2). The superposition of hGSTA3-3·GSH (this work), hGSTA1-1·GSB [PDB accession code 1GUH (*19*)], and hGSTA1-1(R15K)·GSEa [PDB accession code 1GSE (*23*)] indicates that residues 9, 12, 15, 107, 216, and 220 are relatively rigid but residues 10, 111, 208, 213, and 222 are more flexible (Figure 2). For the binding of EA, which is much larger than a phenyl group,

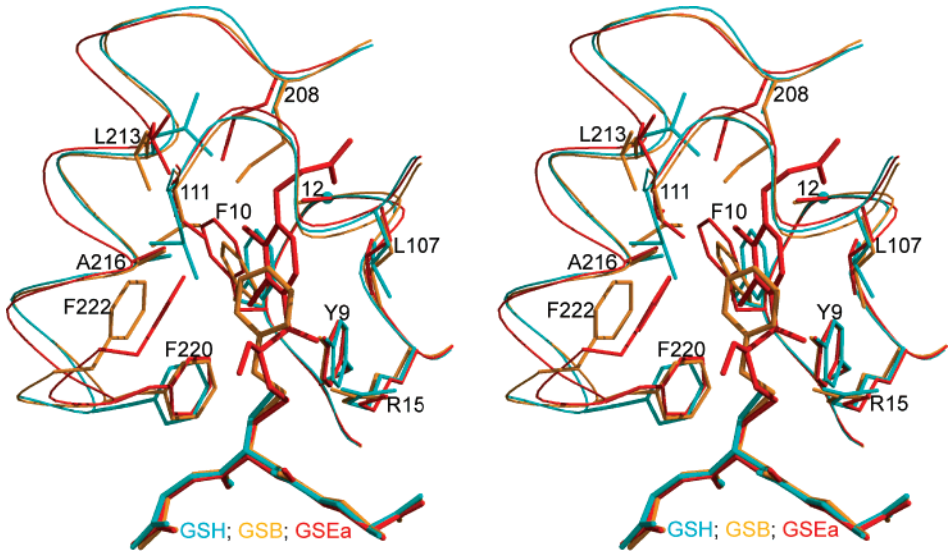

FIGURE 2: Stereoview showing the H-site superposition of human class alpha GSTs. The hGSTA3-3·GSH complex (this work) is in cyan, hGSTA1-1·GSB [PDB accession code 1GUH (*19*)] is in orange, and hGSTA1-1·GSEa [PDB accession code 1GSE (*23*)] is in red. The side chains of H-site defining residues are shown as stick models connected with Cα traces. Conserved residues between hGSTA1-1 and hGSTA3-3 (residues F9, F10, R15, L107, L213, A216, F220, and F222) are labeled with both residue names and numbers, whereas the variants (residues G12, L111, and A208 in hGSTA3, but A12, V111, and M208 in hGSTA1) are labeled with residue numbers only. The illustration was generated with MolScript (*31*) and Raster3D (*30*).

residues 10, 111, 208, 213, and 222 move outward from the H-site (Figure 2). Residues 208, 213, and 222 are located in the last helix of class alpha GST, which is presumably flexible to accommodate the different sizes of xenobiotics. Therefore, the difference between hGSTA1-1 and hGSTA3-3 at position 12 may have more impact than those at positions 111 and 208 on their activities.

Validation of the hGSTA3-3·GSH·Δ^5*-AD Model.* The model of the hGSTA3-3·GSH·Δ^5-AD ternary complex was validated both structurally and functionally. First, Δ^5-AD and EA have similar sizes. The H-site comparison between the hGSTA3-3·GSH·Δ^5-AD model (this work) and the hGSTA1-1·GSEa structure [PDB accession code 1GSE (*23*)] revealed that the Δ^5-AD molecule and the EA moiety occupy almost the same space in the H-site (Figure 3a). Second, to accommodate the difference between Δ^5-AD and the EA moiety of GSEa, F10 and H-site residues located in the last helix undergo significant conformational changes (Figure 3a), in agreement with the fact that the F10 side chain and C-terminal helix undergo significant conformational changes accommodating different ligands (Figure 2). Third, residue 12 is a Gly in hGSTA3-3 but an Ala in hGSTA1-1. The specific activity of wild-type hGSTA3-3 is about 9.5-fold higher than that of wild-type hGSTA1-1 and is reduced by approximately 93% upon G12A mutation (Table 2), which is readily explainable by the closest distance, ~4 Å, between the Cα position of G12 and Δ^5-AD (Figure 3a). Fourth, residue 208 is an Ala in hGSTA3-3 but a Met in hGSTA1-1. Although the closest distance between Cβ of A208 and Δ^5-AD is also ~4 Å, the A208M mutation may not have an impact on catalysis as great as the G12A mutation because residue 208 is located near the flexible C-terminal helix and the side chain of Met is flexible (Figure 2). Indeed, the specific activity of hGSTA3-3 was reduced only slightly upon the A208M mutation (Table 2). The role of amino acid residues in positions 12 and 208 in hGSTA3-3-catalyzed isomerization of Δ^5-AD was further investigated by determining kinetic constants for hGSTA3(G12A) and hGSTA3(A208M) mutants. The kinetic constants for wild-type hGSTA1-1 and hGSTA3-3 were also estimated for direct comparison with the published data (*8*, *13*). As can be seen in Table 3, the kinetic constants for wild-type hGSTA3-3 determined in the present study were comparable to those published by Johnasson and Mannervik (*8*). Even though the kinetic constant for wild-type hGSTA1-1 estimated in the present study was slightly different than the published values (*13*), hGSTA3-3 was a much more efficient catalyst of Δ^5-AD isomerization compared with hGSTA1-1 as previously reported (*8*, *13*). The catalytic efficiency of hGSTA3-3 was reduced by 97% upon the G12A mutation, which was mainly due to an approximate 55% reduction in the V_{max} value and a 18-fold higher K_m for the hGSTA3-3(G12A) mutant compared with wild-type hGSTA3-3. The catalytic efficiency of hGSTA3-3 was also reduced upon A208M mutation, albeit less dramatically compared with the G12A mutation. These results indicated that amino acid residues in position 12 and, to some extent, position 208 affected activity of hGSTA3-3 toward Δ^5-AD. Residue 111 is a Leu in hGSTA3-3, a Val in hGSTA1-1, and a Phe in hGSTA2−2 (*11*). It has been shown that single point mutant hGSTA2-2(F111L) is only 20-fold more active than the wild-type enzyme, which is not significant considering that hGSTA3-3 is 2400-fold more active than hGSTA2-2 (*11*). Consistent with these observations, it has also been shown that hGSTA3-3(L111F) is 27-fold less active than the wild type, which is obviously not significant either (*13*). The little impact of the F111L or L111F mutation is most likely due to the flexible nature of the structural elements where residue 111 is located (Figures 2 and 3a). The L111V mutation is even less dramatic than F111L and, therefore, should not have any significant impact on catalysis. Therefore, we did not characterize the hGSTA3-3(L111V) mutant. Fifth, the binding of Δ^5-AD in the H-site is reasonably good via the electrostatic interactions of its D ring keto group with the A208 amide group and with the R13 guanidinium group and many van der Waals interactions, especially the short contacts

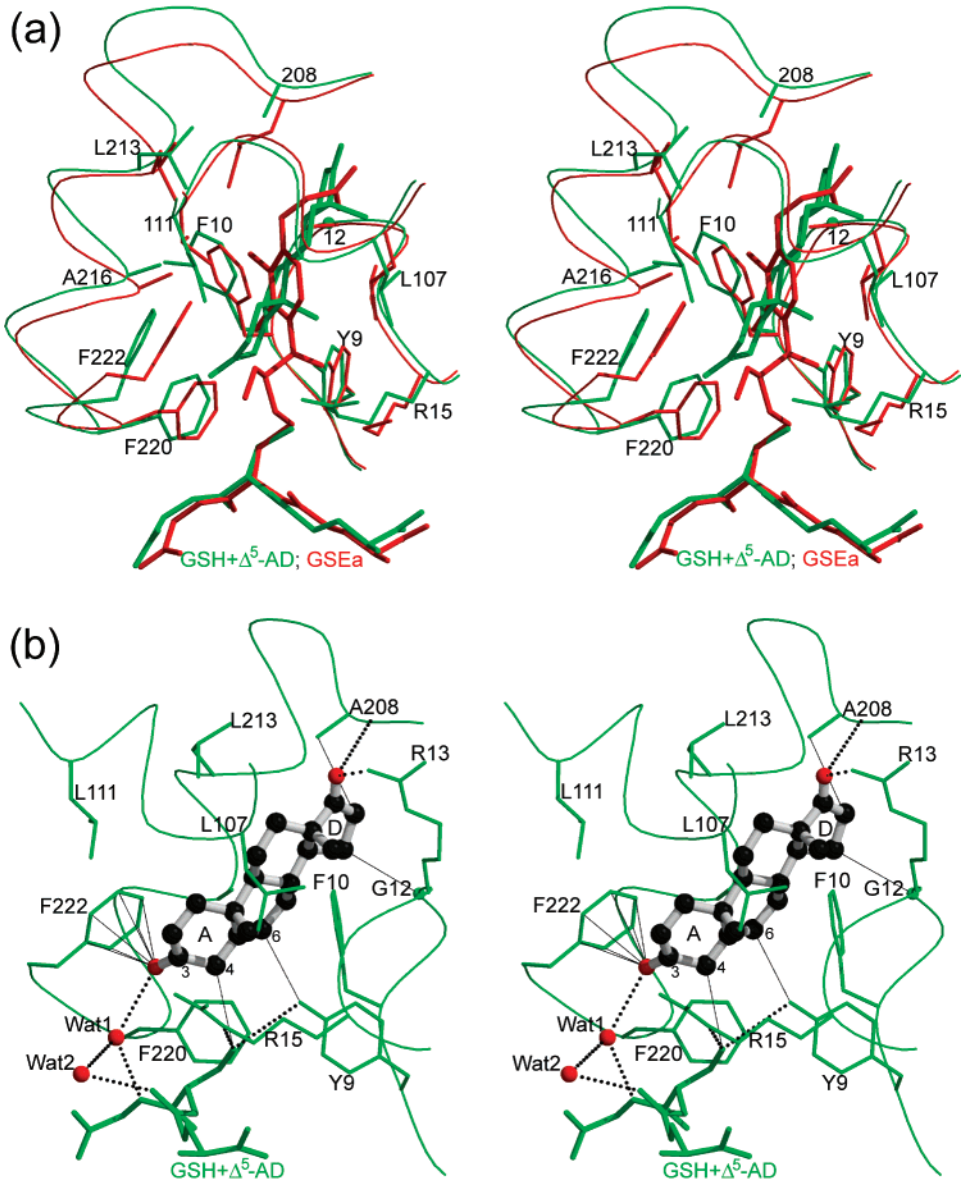

FIGURE 3: Stereoviews illustrating a computer model of the hGSTA3-3·GSH·Δ^5-AD complex. The side chains of H-site defining residues are shown as stick models connected with Cα traces. (a) The H-site superposition of the model (in green, this work) with the crystal structure of hGSTA1-1·GSEa [in red, PDB accession code 1GSE (*23*)]. Conserved residues between hGSTA1-1 and hGSTA3-3 (residues F9, F10, R15, L107, L213, A216, F220, and F222) are labeled with both residue names and numbers, whereas the variants (residues G12, L111, and A208 in hGSTA3, but A12, V111, and M208 in hGSTA1) are labeled with residue numbers only. (b) A different view of hGSTA3-3·GSH·Δ^5-AD showing the detailed interactions between hGSTA3-3 H-site residues (stick model) and the Δ^5-AD molecule (ball-and-stick model with carbon in black and oxygen in red). Residue R13, also conserved between hGSTA1-1 and hGSTA3-3, is shown because of its involvement in the binding of Δ^5-AD. Hydrogen bonds and electrostatic interactions (2.9−3.5 Å) are shown as dotted lines; van der Waals interactions (3.3−4.0 Å) are indicated with solid lines. The illustration was generated with MolScript (*31*) and Raster3D (*30*).

Table 2: Specific Activities [μmol/(min·mg)] of Wild-Type hGSTA1-1 and hGSTA3-3 and Mutants of hGSTA3-3 for Isomerization of Δ^5-AD[a]

hGSTA3-3	hGSTA1-1	hGSTA3(G12A)	hGSTA3(A208M)
104 ± 11	11 ± 0.7	7 ± 1	73 ± 7

[a] Specific activities were determined spectrophotometrically using 100 μM Δ^5-AD and 1 mM GSH at 30 °C in 25 mM sodium phosphate buffer (pH 8). The experiment was repeated three times, and the values shown are the mean ± SE.

of its D ring carbon atoms with G12 and A208 and that between its A ring keto oxygen with the phenyl ring of F222 (Figure 3b). Sixth, the binding mode of Δ^5-AD in the H-site is unique, and Δ^5-AD fits the H-site very well. Significant translation and rotation along the long axis of Δ^5-AD in the H-site is prohibited (Figure 3b). Binding of Δ^5-AD with its hydrophobic ring systems in the solvent channel, which could bring the 3-keto oxygen into the vicinity of the Y9 hydroxyl, is not likely to happen because such binding mode of any substrate of GST has never been observed in any three-dimensional structures. Taken together, we conclude that our hGSTA3-3·GSH·Δ^5-AD model is valid, representing the ternary complex of hGSTA3-3 with both substrate molecules.

Mechanism of the hGSTA3-3-Catalyzed Isomerization Reaction of Δ^5-AD. The mechanism of the hGSTA3-3-catalyzed isomerization of Δ^5-AD is of substantial interest because of its involvement in the production of steroid

Table 3: Kinetic Constants for Wild-Type hGSTA1-1 and hGSTA3-3 and Mutants of hGSTA3-3 for Isomerization of Δ^5-AD[a]

isozyme	V_{max} [μmol/(min·mg)]	K_m (μM)	k_{cat} (s^{-1})	k_{cat}/K_m ($\mu M^{-1}\ s^{-1}$)
hGSTA3(G12A)[b]	45 ± 9	420 ± 124	38 ± 7	0.1 ± 0.02
hGSTA3(A208M)[b]	141 ± 19	83 ± 23	117 ± 15	1.7 ± 0.5
hGSTA1-1[b]	17	78	14	0.18
hGSTA1-1[c]	not reported	58	29	0.5
hGSTA3-3[b]	99	23	83	3.6
hGSTA3-3[d]	not reported	24	102	4.3

[a] Isomerase activity was determined as a function of varying Δ^5-AD concentrations (0.5−100 μM) at a fixed concentration of GSH (1 mM) at 30 °C. Kinetic parameters were estimated by fitting a hyperbolic function to the experimental data points. For mutant enzymes, data are the mean ± SE of three independent experiments. The kinetic constants for wild-type hGSTA1-1 and hGSTA3-3 were also determined for direct comparison with published data. [b] Present study. [c] Data taken from ref *13*. [d] Data taken from Johansson and Mannervik (*8*).

hormones (*8*, *13*). It has been established that the predominant ionization state of the sulfur of GSH in complex with GST is the thiolate and that Y9 plays an important role in the stabilization of the thiolate by serving as a hydrogen bond donor [$GS^-\cdots H-O-Y9$ (*6*)]. Previous studies have also suggested that for efficient catalysis of Δ^5-AD isomerization GSH must be deprotonated and Y9 must be nonionized (*13*). In addition, the ϵ-nitrogen of R15 is within the hydrogen bond distance of the thiolate sulfur of GSH (*19*); each of the atoms N3 and OE1 of GS^- is hydrogen bonded to one or more water molecules, forming a hydrogen bond network [for example, see PDB accession code 1GSE (*23*)]. Our model of hGSTA3-3·GSH·Δ^5-AD suggests that the thiolate sulfur of GS^- is positioned at ~3.5 Å from carbon atom C4, the hydroxyl group of Y9 is ~3.5 Å away from C6, the ϵ-nitrogen of R15 is within the hydrogen bond distance of the thiolate sulfur, and a GSH-bound water molecule may donate a hydrogen bond to the 3-keto group of Δ^5-AD (Figure 3b). Accordingly, we propose a reaction mechanism as outlined in Figure 4. In this mechanism, the thiolate of GS^- is stabilized by R15, and the isomerization reaction is initiated by the formation of a double bond between C3 and C4 involving two concerted changes: the formation of a hydrogen bond between the GSH-bound water molecule and the 3-keto oxygen and the transfer of a proton from C4 to GS^- (Figure 4a), resulting in the formation of the dienolate intermediate of the reaction (Figure 4b). The conjugate system O3−C3−C4−C5−C6 of the dienolate allows the negative charge to move easily from O3 to C6, and it is also feasible for the protonated GSH to donate a hydrogen bond to the hydroxyl group of Y9. Thus the hydroxyl hydrogen of Y9 will be readily transferred to the negatively charged C6 (Figure 4c), resulting in the formation of Δ^4-AD (Figure 4d). Finally, the proton of GSH is transferred to the ionized hydroxyl group of Y9, and the active center is ready for the next round of catalysis after Δ^4-AD is replaced with another Δ^5-AD (Figure 4e).

On the basis of in-depth enzymology and mutagenesis studies, Johansson and Mannervik previously proposed a mechanism for the hGSTA3-3-catalyzed Δ^5-AD isomerization reaction (*13*). Using our structure of hGSTA3-3·GSH in combination with available structures of hGSTA1-1, we have constructed a model of hGSTA3-3·GSH·Δ^5-AD (Figures 3), which has additional mechanistic implications. The two mechanisms share the same feature that the thiolate of GS^- serves as the base to withdraw a proton from atom C4 of Δ^5-AD. The major difference between the two mecha-

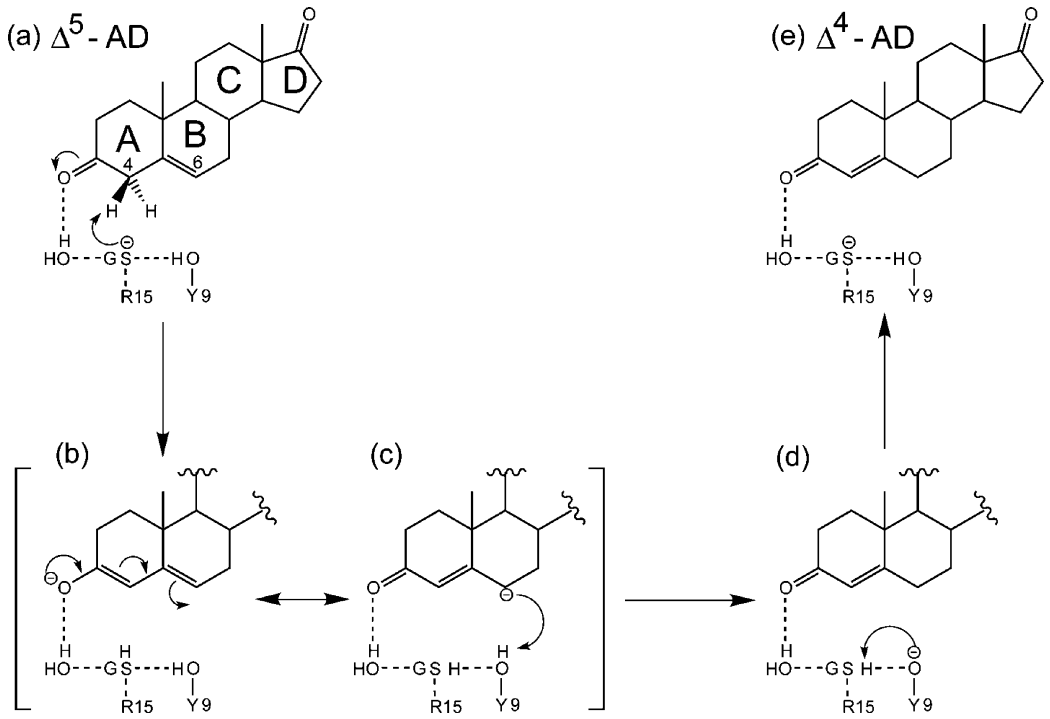

FIGURE 4: Proposed mechanism for the isomerization reaction of Δ^5-AD catalyzed by hGSTA3-3. (a) The isomerization reaction is initiated by the formation of a double bond between C3 and C4, which is enabled by the formation of a hydrogen bond between an GSH-bound water molecule and the 3-keto oxygen and the transfer of a proton from C4 to GS^-, resulting in the formation of (b) the dienolate. The conjugate system O3−C3−C4−C5−C6 of the dienolate allows the negative charge to move easily from O3 to C6 (c), ready to accept the proton provided by the hydroxyl group of Y9, resulting in the formation of Δ^4-AD. (d) Finally, the proton of GSH is transferred to the ionized hydroxyl group of Y9, and (e) the active center is ready for the next round of catalysis after Δ^4-AD is replaced with another Δ^5-AD.

nisms resides in the role of the Y9 hydroxyl. In the previously proposed mechanism, the Y9 hydroxyl donates a hydrogen bond to the 3-keto oxygen of the substrate and thus stabilizes the reaction intermediate (*13*). In our model of hGSTA3-3·GSH·Δ^5-AD, not only the distance (~6.0 Å) between the Y9 hydroxyl and 3-keto oxygen but also the spatial arrangement of the two groups makes the formation of this hydrogen bond impossible (Figure 3b). Instead, our model suggests that the Y9 hydroxyl group functions with GS^- in a concerted manner to transfer a proton from C4 to C6 (Figure 3b). The single mutation that produces the most pronounced difference in specific activity with Δ^5-AD is the Y9F mutation, which lowers the specific activity 350-fold (*13*), indicating a much more important role of the Y9 hydroxyl than just donating a hydrogen bond to the 3-keto oxygen. In our mechanism, the role of donating a hydrogen bond to the 3-keto group and thus stabilizing the reaction intermediate is fulfilled by a GSH-bound water molecule (Figures 3b and 4), whereas the Y9 hydroxyl group is directly involved in the proton transfer.

Proton transfer is optimal when the proton-conducting wire involves the GS^- thiolate and Y9 hydroxyl (Figure 4). However, when a portion of the wire or the entire wire is missing, the proton transfer should still be possible, but much less efficient. In such situation, the hydrogen bond network of water molecules can, to some extent, substitute for the missing elements of the proton-conducting wire.

ACKNOWLEDGMENT

We thank Drs. Jianhua Gan and Hehua Liu for insightful discussions.

REFERENCES

1. Sheehan, D., Meade, G., Foley, V. M., and Dowd, C. A. (2001) Structure, function and evolution of glutathione transferases: implications for classification of non-mammalian members of an ancient enzyme superfamily, *Biochem. J. 360*, 1−16.
2. Dixon, D. P., Lapthorn, A., and Edwards, R. (2002) Plant glutathione transferases, *GenomeBiology 3*, REVIEWS3004.
3. Armstrong, R. N. (1991) Glutathione *S*-transferases: reaction mechanism, structure, and function, *Chem. Res. Toxicol. 4*, 131−140.
4. Armstrong, R. N. (1994) Glutathione *S*-transferases: structure and mechanism of an archetypical detoxication enzyme, *Adv. Enzymol. Relat. Areas Mol. Biol. 69*, 1−44.
5. Hayes, J. D., and Pulford, D. J. (1995) The glutathione *S*-transferase supergene family: regulation of GST and the contribution of the isoenzymes to cancer chemoprotection and drug resistance, *Crit. Rev. Biochem. Mol. Biol. 30*, 445−600.
6. Armstrong, R. N. (1997) Structure, catalytic mechanism, and evolution of the glutathione transferases, *Chem. Res. Toxicol. 10*, 2−18.
7. Dirr, H., Reinemer, P., and Huber, R. (1994) X-ray crystal structures of cytosolic glutathione *S*-transferases. Implications for protein architecture, substrate recognition and catalytic function, *Eur. J. Biochem. 220*, 645−661.
8. Johansson, A. S., and Mannervik, B. (2001) Human glutathione transferase A3-3, a highly efficient catalyst of double-bond isomerization in the biosynthetic pathway of steroid hormones, *J. Biol. Chem. 276*, 33061−33065.
9. Kuliopulos, A., Mildvan, A. S., Shortle, D., and Talalay, P. (1989) Kinetic and ultraviolet spectroscopic studies of active-site mutants of delta 5−3-ketosteroid isomerase, *Biochemistry 28*, 149−159.
10. Benson, A. M., Talalay, P., Keen, J. H., and Jakoby, W. B. (1977) Relationship between the soluble glutathione-dependent delta 5−3-ketosteroid isomerase and the glutathione *S*-transferases of the liver, *Proc. Natl. Acad. Sci. U.S.A. 74*, 158−162.
11. Pettersson, P. L., Johansson, A. S., and Mannervik, B. (2002) Transmutation of human glutathione transferase A2-2 with peroxidase activity into an efficient steroid isomerase, *J. Biol. Chem. 277*, 30019−30022.
12. Pettersson, P. L., and Mannervik, B. (2001) The role of glutathione in the isomerization of delta 5-androstene-3,17-dione catalyzed by human glutathione transferase A1-1, *J. Biol. Chem. 276*, 11698−11704.
13. Johansson, A. S., and Mannervik, B. (2002) Active-site residues governing high steroid isomerase activity in human glutathione transferase A3-3, *J. Biol. Chem. 277*, 16648−16654.
14. Pal, A., Pan, S.-S., and Singh, S. V. (2002) Activity of alpha class human glutathione transferase isoenzymes for glutathione conjugation of (+)-anti-7,8-dihydroxy-9,10-oxy-7,8,9,10-tetrahydrobenzo[*a*]pyrene, *Proc. Am. Assoc. Cancer Res. 43* (Suppl.), 691.
15. Zhao, T., Singhal, S. S., Piper, J. T., Cheng, J., Pandya, U., Clark-Wronski, J., Awasthi, S., and Awasthi, Y. C. (1999) The role of human glutathione *S*-transferases hGSTA1-1 and hGSTA2-2 in protection against oxidative stress, *Arch. Biochem. Biophys. 367*, 216−224.
16. Xia, H., Pan, S. S., Hu, X., Srivastava, S. K., Pal, A., and Singh, S. V. (1998) Cloning, expression, and biochemical characterization of a functionally novel alpha class glutathione *S*-transferase with exceptional activity in the glutathione conjugation of (+)-anti-7,8-dihydroxy-9,10-oxy-7,8,9,10-tetrahydrobenzo[*a*]pyrene, *Arch. Biochem. Biophys. 353*, 337−348.
17. Otwinowski, Z., and Minor, W. (1997) Processing of X-ray diffraction data collected in oscillation mode, *Methods Enzymol. 276*, 307−326.
18. Navaza, J. (1994) An automated package for molecular replacement, *Acta Crystallogr. A 50*, 157−163.
19. Sinning, I., Kleywegt, G. J., Cowan, S. W., Reinemer, P., Dirr, H. W., Huber, R., Gilliland, G. L., Armstrong, R. N., Ji, X., Board, P. G., Olin, B., Mannervik, B., and Jones, T. A. (1993) Structure determination and refinement of human alpha class glutathione transferase A1-1, and a comparison with the Mu and Pi class enzymes, *J. Mol. Biol. 232*, 192−212.
20. Brünger, A. T., and Rice, L. M. (1997) Crystallographic refinement by simulated annealing: methods and applications., *Methods Enzymol. 277*, 243−269.
21. Jones, T. A., and Kjeldgaard, M. (1997) Electron-density map interpretation, *Methods Enzymol. 277*, 173−208.
22. Ha, N. C., Kim, M. S., Lee, W., Choi, K. Y., and Oh, B. H. (2000) Detection of large pK_a perturbations of an inhibitor and a catalytic group at an enzyme active site, a mechanistic basis for catalytic power of many enzymes, *J. Biol. Chem. 275*, 41100−41106.
23. Cameron, A. D., Sinning, I., L'Hermite, G., Olin, B., Board, P. G., Mannervik, B., and Jones, T. A. (1995) Structural analysis of human alpha-class glutathione transferase A1-1 in the apo-form and in complexes with ethacrynic acid and its glutathione conjugate, *Structure 3*, 717−727.
24. Brünger, A. T., Adams, P. D., Clore, G. M., DeLano, W. L., Gros, P., Grosse-Kunstleve, R. W., Jiang, J. S., Kuszewski, J., Nilges, M., Pannu, N. S., Read, R. J., Rice, L. M., Simonson, T., and Warren, G. L. (1998) Crystallography & NMR system: A new software suite for macromolecular structure determination, *Acta Crystallogr. D 54*, 905−921.
25. Powell, M. J. D. (1977) Restart procedures for the conjugate gradient method, *Math. Prog. 12*, 241−254.
26. Engh, R. A., and Huber, R. (1991) Accurate bond and angle parameters for X-ray protein structure refinement, *Acta Crystallogr. A 47*, 392−400.
27. Laskowski, R. A., MacArthur, M. W., Moss, D. S., and Thornton, J. M. (1993) PROCHECK: a program to check stereochemical quality of protein structures, *J. Appl. Crystallogr. 26*, 283−291.
28. Gu, Y., Singh, S. V., and Ji, X. (2000) Residue R216 and catalytic efficiency of a murine class alpha glutathione *S*-transferase toward benzo[*a*]pyrene 7(*R*),8(*S*)-diol 9(*S*),10(*R*)-epoxide, *Biochemistry 39*, 12552−12557.
29. Esnouf, R. M. (1997) An extensively modified version of MolScript that includes greatly enhanced coloring capabilities, *J. Mol. Graphics Modell. 15*, 132−134.
30. Merritt, E. A., and Bacon, D. J. (1997) Raster3D: photorealistic molecular graphics, *Methods Enzymol. 277*, 505−524.
31. Kraulis, P. J. (1991) MOLSCRIPT: a program to produce both detailed and schematic plots of protein structures, *J. Appl. Crystallogr. 24*, 946−950.

BI048757G